Available online at www.sciencedirect.com
SCIENCE DIRECT
Biochemical and Biophysical Research Communications 339 (2006) 157–164
BBRC
www.elsevier.com/locate/ybbrc

The crystal structure of an odorant binding protein from *Anopheles gambiae*: Evidence for a common ligand release mechanism ☆,☆☆

Mark Wogulis [a], Tania Morgan [b], Yuko Ishida [b], Walter S. Leal [b], David K. Wilson [a,*]

[a] *Section of Molecular and Cellular Biology, University of California, Davis, CA 95616, USA*
[b] *Department of Entomology, University of California, Davis, CA 95616, USA*

Received 19 October 2005
Available online 9 November 2005

Abstract

The *Anopheles gambiae* mosquito is the main vector of malaria transmission in sub-Saharan Africa. We present here a 1.5 Å crystal structure of AgamOBP1, an odorant binding protein (OBP) from the *A. gambiae* mosquito. The protein crystallized as a dimer with a unique binding pocket consisting of a continuous tunnel running through both subunits of the dimer and occupied by a PEG molecule. We demonstrate that AgamOBP1 undergoes a pH dependent conformational change that is associated with reduced ligand binding. A predominance of acid-labile hydrogen bonds involving the C-terminal loop suggests a mechanism in which a drop in pH causes C-terminal loop to open, leaving the binding tunnel solvent exposed, thereby lowering binding affinity for ligand. Because proteins from two distantly related insects also undergo a pH dependent conformational change involving the C-terminus that is associated with reduced ligand affinity, our results suggest a common mechanism for OBP activity.

Keywords: *Anopheles gambiae*; Olfaction; Crystal structure; Ligand binding; pH dependent binding; Malaria

Olfactory stimulus plays a major role in insect behaviors such as host-seeking, oviposition, and mating. For example, female *Anopheles gambiae* mosquitoes, which are the main vectors of malaria transmission in sub-Saharan Africa, use olfactory cues to find human hosts and avoid non-human hosts [1]. It is therefore of interest to better understand the olfactory system of mosquitoes and other insects in the hopes of disrupting undesirable host-insect interactions.

Considerable progress has been made in understanding insect olfaction, and it is known that odorant binding proteins (OBPs) and odorant receptors (ORs) play important roles [2]. This system has been most fruitfully studied in pheromone detection, where there are clear behavioral responses that can be measured, and where the chemicals that elicit these responses have been identified. It is clear that pheromones bind to pheromone binding proteins (PBP) [3,4], a functional subclass of OBPs, which are highly abundant in insect antennae and that ORs on the olfactory receptor neurons are activated directly or indirectly by pheromones [5]. In addition, it has been shown that there are odorant degrading enzymes (ODEs) that quickly clear odorant to allow for response to rapid changes in odorant concentrations as insects navigate toward the source [6–8].

It is clear from several lines of evidence that OBPs play some role in behavioral responses to odorants, such as pheromones [7,9–14]. One hypothesis holds that, analogous to bacterial chemical sensory mechanisms, binding of an odorant to OBP leads to a conformational change in the odorant binding protein which is then detected by the OR [15]. An alternate hypothesis holds that odorants bind directly to ORs and that the function of OBPs is to protect the odorants from degradation by ODEs [16]. In

☆ Coordinates have been deposited into the Protein Data Bank under accession number 2ERB.
☆☆ *Abbreviations:* AgamOBP1, *Anopheles gambiae* OBP; Apo1PBP1, *Antheraea polyphemus* pheromone binding protein; LmaPBP, *Leucophaea maderae* pheromone binding protein; LUSH, *Drosophila* odorant binding protein; OBP, odorant binding protein; OR, odorant receptor; PBP, pheromone binding protein.

* Corresponding author. Fax: +1 530 752 3085.
E-mail address: dave@alanine.ucdavis.edu (D.K. Wilson).

0006-291X/$ - see front matter © 2005 Elsevier Inc. All rights reserved.
doi:10.1016/j.bbrc.2005.10.191

addition, or instead, the function of the OBP may be to solubilize highly hydrophobic odorants [3], though in some cases, as with the cockroach *Leucophaea maderae*, the pheromone is water soluble on its own [17]. In either case, OBPs will function to deliver odorants to ORs, which in turn are activated directly by the odorant [13].

Structural evidence for the latter hypothesis was provided by a pair of structures of the PBP from *Bombyx mori*. The crystal structure of the *B. mori* PBP–bombykol complex (in pH 8.2 buffer) showed a 6 helix globular protein with the pheromone bombykol ((*E*,*Z*)-10,12-hexadecanedienol) bound in a hydrophobic binding pocket [18]. Most interestingly, the NMR structure showed that at pH lower than 4.9, a seventh helix forms which occupies the hydrophobic pocket, thus precluding binding of the pheromone at a low pH [19]. In vitro, *B. mori* PBP has been shown to bind bombykol at neutral, but not acidic pH. Studies have shown that the membrane surface around the OR in insect antennae is negatively charged [20], which induces a drop in pH immediately around the membrane surface. It appears, therefore, that *B. mori* PBP transports bombykol to the membrane surface, where it encounters a low pH and releases the bombykol [19]. The free bombykol would then be able to bind to OR. In support of this hypothesis, it has been demonstrated the artificial anionic lipids are sufficient to cause *B. mori* PBP to release bound bombykol, while artificial neutral lipids are not sufficient [21]. It has also been demonstrated that OR from *Drosophila* and from *B. mori* expressed in *Xenopus* can be activated by odorant alone [5,22].

Aside from *B. mori* PBP, structures of four more OBPs have been published from *Drosophila* (LUSH), cockroach *L. maderae* (LmaPBP), the honeybee *Apis mellifera* (Amel-ASP1), and the giant silk moth *Antheraea polyphemus* (ApolPBP1) [17,23–25]. These proteins are structurally homologous to the *B. mori* PBP. All contain helices, and three disulfide bridges which connect the helices in a similar manner. Thus, the overall topology of these four structures is essentially identical. The structures differ in the relative distances between the helices, the lengths and positions of loops connecting the helices and the lengths of C and N-terminal loops. The nature and shape of the binding pockets also differ, presumably reflecting the different specificities for odorants. Significantly, of the five structures, only the Lepidopteran *B. mori* PBP and ApolPBP1 have a C-terminal tail long enough to form a helix that would fit into the binding pocket. ApolPBP1 also undergoes a pH dependent conformational change that is associated with a loss of ligand binding at low pH [25,26]. This seemed to suggest that the mechanism of odorant release differed in *B. mori* PBP and ApolPBP1 from that of the other three proteins. This further suggested that perhaps the hypothesis that OBPs serve as carrier proteins delivering their cargo to ORs in response to a drop in pH might not be generally true for OBPs, which do not all have this C-terminal extension.

Recently, in an effort to further understand olfactory sensing in the mosquito *A. gambiae*, a search for OBPs from this species was carried out by isolating mRNAs that were abundantly and specifically expressed in mosquito antennae. These were screened to determine which had size and amino acid sequence characteristics of OBPs. Seven putative *A. gambiae* OBPs were discovered from this screen, all of which were found in both male and female antennae [27].

We have expressed and crystallized purified protein of one of these OBPs, AgamOBP1, and determined its 1.5 Å crystal structure. This protein crystallized as a dimer in the asymmetric unit. This dimer has an unusual binding pocket, which consists of a single tunnel running through both molecules. There was a serendipitous ligand in the tunnel, which we have identified as PEG, which was used as a precipitant to induce crystallization of the protein. While the native ligand of AgamOBP1 has not been identified, we have demonstrated that AgamOBP1 undergoes a pH dependent conformational change which is associated with a diminished capacity for binding a non-native ligand. The structure suggests that several acidic residues that connect the N and C termini of this protein may play a role in the reduction of binding by allowing these termini to unfold at low pH, thereby exposing the ligand to solvent. Together, these data suggest that the ability to release ligand on pH reduction may not be limited to *B. mori* PBP but rather be a more general feature of OBPs.

Materials and methods

Protein expression and purification. Protein was produced using *Escherichia coli* BL21(DE3) transformed with a pET-22 b(+) periplasmic expression vector containing AgamOBP1 cDNA sequence, essentially as previously described for *B. mori* PBP [21]. Recombinant protein, identical in sequence to that of secreted native AgamOBP1, was purified by ion exchange chromatography and gel filtration. Ion exchange was first carried out on a Q-Sepharose column with a 0–500 mM NaCl gradient, followed by the first mono-Q gradient: 0–300 mM NaCl. A Superdex75 size exclusion column was run, with an earlier eluting peak containing AgamOBP1 dimer and a later peak containing monomer. The monomeric fraction was then further purified on a Mono-Q column, with a 0–250 mM NaCl gradient, followed by a third Mono-Q column eluted with 0–300 mM. The purest AgamOBP1 fractions were pooled, desalted into water with a HiTrap column, and concentrated to 100 mg/ml in a Amicon 5 kDa cutoff concentrator. The mass of the protein was confirmed through electrospray ionization mass spectroscopy. The selenomethionine preparation was done similarly, except that the cultures were inoculated into minimal media. After growing to log phase, temperature was dropped to 15 °C. One hundred milligram per liter of lysine, phenylalanine, and threonine, and 50 mg/L isoleucine, leucine, and valine were added to suppress methionine biosynthesis. After 30 min., selenomethionine was added at 60 mg/L. Fifteen minutes after adding selenomethionine, cells were induced with 0.24 mM IPTG and induced overnight at 15 °C. Mass spectroscopy measurements on purified SeMet AgamOBP1 indicated that all four methionines had been completely replaced with selenomethionine.

Crystallization and data collection. Purified protein was concentrated to 100 mg/ml in deionized water. Crystals were formed by the hanging drop method. One microliter of protein was mixed with 1 μl well buffer, consisting of 32% PEG 8000, 250 mM $MgCl_2$, 50 mM Tris–HCl, pH 8.0. Crystals were harvested and cooled to 100 K using well buffer as a

cryoprotectant. Data were collected at beamline 9–2 at the Stanford Synchrotron Radiation Laboratory. Selenomethionine data were collected to 2.0 Å at peak, inflection, and remote wavelengths. A native dataset was collected to 1.5 Å at a wavelength of 0.88557 Å. Both datasets indicated crystals in the $P2_1$ spacegroup. However, the native dataset had unit cell dimensions of $a = 30.1$ Å, $b = 68.2$ Å, $c = 61.5$ Å, $\alpha = \gamma = 90°$, and $\beta = 99.77°$, while the selenomethione dataset had unit cell dimensions of $a = 59.7$ Å, $b = 68.1$ Å, $c = 63.6$ Å, $\alpha = \gamma = 90°$, and $\beta = 109.6°$. This difference in unit cell dimensions did not seem to be due only to the presence of selenomethionine, since some native crystals had the larger unit cell as well.

Structure determination. Exhaustive efforts to phase a native dataset by molecular replacement, using the programs EPMR [28], Phaser [29], and Amore [30], with any of the four previously solved OBP structures (alone or in combination) failed. Native data were integrated and scaled using the program MOSFLM [31]. Data collected from selenomethionine crystals were integrated using the program MOSFLM and then scaling, and initial phase calculation was done using the program Solve, yielding a figure of merit of 0.36 [32]. Phases were improved using Resolve (figure of merit = 0.78) [32] which automatically built 223 alanine and glycine residues. The resulting density clearly showed four molecules per asymmetric unit. The AgamOBP1 sequence was manually built into the density of one molecule using the program O [33]. The native dataset had two molecules per asymmetric unit and two molecular replacement solutions for the native dataset were found by the program Phaser using the monomer as a search model. The model was refined by several rounds of simulated annealing followed by positional refinement using the program CNS [34]. Final adjustments were done manually, with water molecules added using CNS. One Mg^{2+} ion (coordinating six water molecules) was clearly visible and modeled in. Unexplained continuous electron density in the binding pocket was interpreted as PEG and was modeled in by hand using the program O and refined using positional refinement in CNS. PDB, topology, and parameter files for PEG were generated by the PRODRG website [35]. The final structure consisted of residues 3–125 of each monomer, 431 water molecules, one Mg^{2+} ion, and one PEG molecule of 28 ethylene glycol subunits. Ser117 from both chains A and B, as well as Glu43 and Met 89 from chain A, showed alternate conformations of side chain atoms. In all five cases, each conformation was set to an occupancy of 50% and refined. Ramachandran statistics were calculated with the program Procheck [36]. Buried surface area was calculated using the program CNS. RMS deviations were calculated with the program LSQKAB [37]. All figures were generated using the program PyMol (DeLano Scientific, LLC).

Protein extraction and mass spectroscopy analysis. A sample of the same batch of protein used to make crystals was extracted by mixing 200 μl of 1 mg/ml aqueous solution of AgamOBP1 with 25 μl sodium formate, pH 3, and 50 μl of distilled hexane. Control sample had double-distilled water instead of the protein. Samples were vortexed for 30 s and then centrifuged at 1240 × g for 7 min and analyzed by GC–MS.

Circular dichroism spectroscopy. Circular dichroism spectra were obtained on a JASCO J-810 spectrophotometer essentially as described previously [21]. Measurements were taken at pH 7.0 and pH 5.5, both above the theoretical p*I* of 5.4.

Binding assay. Binding of 64 μM bombykol ((*E*,*Z*)-10,12-hexadecadienol) to 100 μg/ml AgamOBP1 in either 100 mM ammonium acetate, pH 7, or 100 mM sodium acetate, pH 5.0, was done as previously described [3].

Results

Overall structure

The structure of OBP from *A. gambiae* was determined by X-ray diffraction to a resolution of 1.5 Å. Initial phases were determined using a MAD dataset from crystals from a seleno-methionine preparation of AgamOBP1. A crude initial model was built using these data, and this model was then used to phase the native dataset. Electron density for the protein was quite clear and produced a structure with a final R_{cryst} of 16.9% and R_{free} of 20.2% (Table 1). The overall fold of six helices connected by loops and containing a hydrophobic binding pocket is similar to seen in five other OBPs whose structures have been determined. The three conserved disulfide bonds are also present and are structurally conserved (Fig. 1). Despite the similarity of the overall fold, there were significant differences between AgamOBP1 and the five other OBPs whose three-dimensional structures have been determined. An LSQKAB alignment using the alpha carbons of only the

Table 1
Data collection and structure refinement statistics for AgamOBP1

	Native	SeMet		
		λ1 (peak)	λ2 (remote)	λ3 (inflection)
Data collection statistics				
Wavelength (Å)	0.88557	0.97922	0.81914	0.97936
Resolution (Å) (highest shell)	30–1.5 (1.54–1.50)	100–2.0 (2.11–2.0)	100–2.0 (2.11–2.0)	100–2.0 (2.11–2.0)
Reflections (observed/unique)	147,410/39,190	182,673/32,651	183,843/32,640	182,906/32,649
Completeness (%)	99.9 (100)	100 (100)	100 (100)	100 (100)
$I/\sigma(I)$	11.0 (3.1)	11.1 (5.4)	12.7 (5.9)	11.9 (5.3)
R_{merge}	0.038 (0.133)	0.132 (0.393)	0.120 (0.366)	0.131 (0.458)
Refinement statistics				
Resolution (Å)	30–1.5			
R_{cryst} (%)	16.9			
R_{free} (%)	20.2			
r.m.s.d. bond lengths (Å)	0.0098			
r.m.s.d. bond angles (°)	1.51			
Ramachandran plot				
% in most favorable regions	92			
% in allowed regions	8.0			

Parentheses indicate values for the high resolution shell.

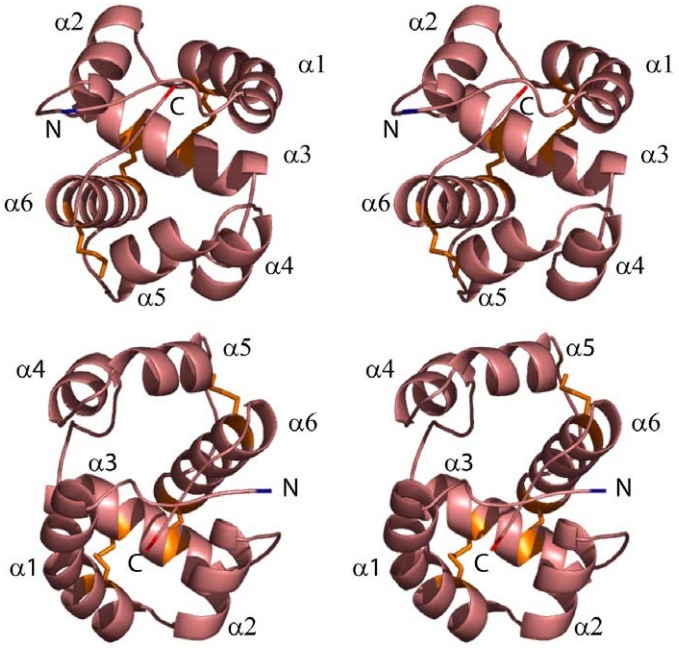

Fig. 1. Three-dimensional structure of AgamOBP1. Stereo view of AgamOBP1 dimer in cartoon representation. The N and C termini and the six helices are labeled. In addition, the N-terminus is shown in blue, the C-terminus in red, and the three disulfide linkages are orange stick representations.

74 residues of the 6 helices showed an RMSD from AgamOBP1 of 4.2 Å for ApolPBP1, 2.4 Å for *B. mori* PBP, 2.3 Å for LmaPBP, 1.6 Å for LUSH, and 1.7 Å for Amel-ASP1. Sequence conservation is very low between AgamOBP1 and these other proteins ranging from 12% to 24% identity. There were also significant differences in the loops connecting these helices, but insertions and deletions in these loops relative to AgamOBP1 made a meaningful RMSD comparison of the loops in these six structures difficult.

The pheromone binding protein from *A. mellifera* has the closest primary sequence similarity to AgamOBP1. However, both *Drosophila melanogaster* and *A. gambiae* belong to the order Diptera, and so are evolutionarily the most closely related organisms among these six. In all three of these most closely related structures, the C-terminal loop makes up part of the wall of the binding pocket, with the C-terminal residue abutting the first helix (Fig. 2). In AgamOBP1, the C-terminal carboxylate oxygens are within hydrogen bonding distance of the hydroxyl of Tyr54 and of the δ nitrogen of His23. This is in contrast to LmaPBP and ApolPBP1 in which the C-terminal residues do not touch the first helix at all, and to PBP from *B. mori*, in which the C-terminal strand does make contact with the first helix, but the C-terminal carboxylate is solvent exposed and makes no contact with the first helix. The N-terminal residues differ between these three most closely related structures. In the case of LUSH, the N-terminal amino acid is a part of the first helix. In Amel-ASP1, as in AgamOBP1, there is an N-terminal loop leading into the helix. In both cases, this loop contacts the C-terminal loop that makes up part of the binding pocket wall. However, the N-terminal extension of AgamOBP1 is six residues longer than that of Amel-ASP1.

Dimer interface

Gel purified AgamOBP1 elutes from the column in two peaks, which correspond to monomer and dimer fractions, with the majority being in the monomer fraction. These fractions interconvert over time (data not shown), and the fraction that was used for these crystallization studies was the monomeric fraction. Despite starting as a monomer, the native protein crystals contained two protein molecules per asymmetric unit, and the selenomethionine protein contained four. The dimeric interface of the native protein is formed across the noncrystallographic twofold axis and primarily engages the fourth and fifth helices, and the loop that is C-terminal to the fifth helix. These contacts bury 1212 $Å^2$ of surface area. The non-polar side chains making up the contact are Leu73, Leu96, and Met89, as well as non-polar atoms in His72 and His90. The remaining contacts are polar and involve the side

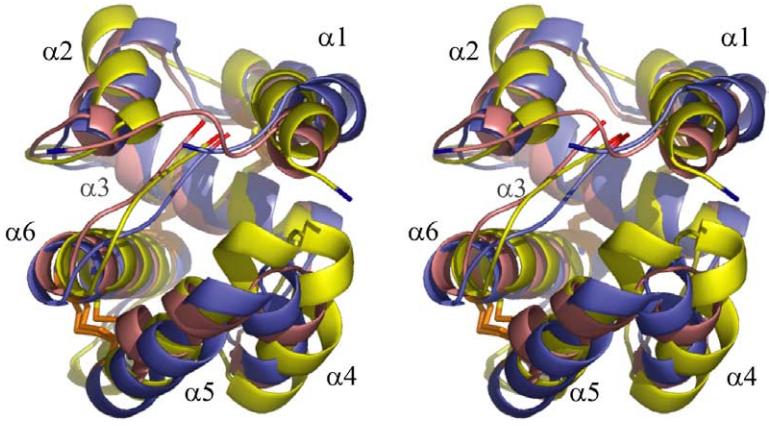

Fig. 2. Comparison of three related OBP structures. Stereo view of overlay of one dimer each of AgamOBP1 (salmon, as in Fig. 1), Amel-ASP1 (blue), and LUSH (yellow). Coloring of N and C termini and disulfides is the same as in Fig. 1.

chains of Glu74, His77, Asp78, Lys93, Arg94, Leu96, and Tyr97, and the main chain atoms of Leu73 and Leu96. The large surface area of the interface suggests that the dimer is not due strictly to crystal packing. However, the presence of so few hydrophobic side chains in the interface (about 50% of the interface is due to hydrophobic atoms) suggests that AgamOBP1 is more likely a monomer in vivo.

The LUSH crystal structures at pH 4.6 (with ethanol, *n*-propanol, and *n*-butanol bound) show a dimer in the asymmetric unit. This dimer buries an interface of 1280 Å^2 [24]. Despite the structural similarities between LUSH and AgamOBP1, the buried interfaces are in different locations, with the LUSH interface being largely due to symmetrical contacts between helices 1 and 2 of each molecule and the AgamOBP1 interface being due largely to symmetrical contacts between helices 4 and 5 of each molecule. The other three structurally characterized OBPs all had either no obvious dimeric interfaces or had only small surface areas buried.

Binding pocket

The most unusual feature of AgamOBP1 relative to the other five OBP structures is its binding pocket. Unlike the other structures, which have a single entrance (though in the case of *B. mori* PBP, it is not entirely clear how the pheromone enters the protein) that opens up into a larger binding pocket or are monomers, AgamOBP1 has one continuous channel running from one side of one molecule, through the dimeric interface, and then out through the second molecule of the dimer (Fig. 3A).

While solving the structure of AgamOBP1, it became clear that there was unexplained density running through the binding channel of the protein. Several possibilities existed to account for this: (1) a water channel, (2) endogenous lipids from the bacterial expression host, and (3) PEG from the crystallization conditions. Water is unlikely because the $2F_o-F_c$ density is unbroken for a very large distance (roughly 30 Å) through a hydrophobic tunnel (Fig. 3B). To determine whether a host-derived compound from the protein expression and purification were the source of the density, protein from the batch used to form the crystals was concentrated, extracted, and analyzed by GC–MS. The only reasonably significant amount of contaminant found was of oleimide (amidated oleic acid) (data not shown). This was found in low concentrations and despite attempts to model it, it was not consistent with the density. On the other hand, PEG was present at high concentrations (well buffer contained 32% PEG 8K) and a short PEG molecule fit the density very well (Fig. 3B). Furthermore, PEG could be modeled so as to provide polar contacts between the oxygen atoms in PEG and ordered water near the opening of the binding pocket (Fig. 3C). Oleimide could not be positioned so as to provide hydrogen bonding contacts with that water. Thus, the high concentration of PEG in the crystallization conditions, the ability to fit PEG into the electron density, and the absence of other alternate ligands all lead to the conclusion that PEG is highly likely to be the ligand, although it is impossible to definitively exclude all other possibilities.

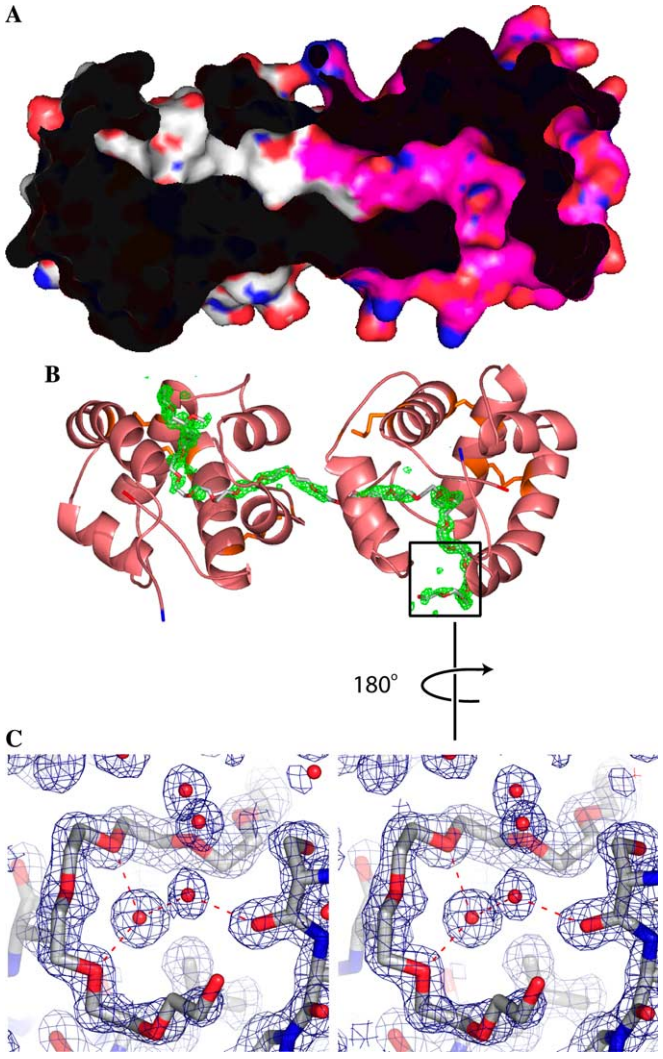

Fig. 3. AgamOBP1 binding pocket consists of a single, long tunnel running through the dimer. (A) Cutaway view of a surface representation of the AgamOBP1 dimer. Carbon atoms of monomer A are in magenta and those of monomer B are in white. All oxygen atoms are in red and nitrogen atoms in blue. PEG ligand was removed to generate the surface representation. (B) An F_o–F_c map contoured at 3σ phased without any ligand modeled in. The map was contoured around the PEG model. One PEG molecule (consisting of 28 ethylene glycol subunits) is shown passing through one AgamOBP1 dimer. (C) Boxed area shown in (B) was rotated approximately 180° and is shown closeup in stereo view with the final refined $2F_o$–F_c map. Hydrogen bonds involving the PEG molecule are shown by red dotted lines.

The surface of the binding pocket is largely hydrophobic. In fact, the PEG ligand makes only hydrophobic contacts through the whole length of the dimer and makes polar contacts with the protein only through ordered water molecules, and even then, only in a limited number of places. Polar atoms from the side chains of Tyr10, Ser79, His111, and Trp114 are exposed to the binding pocket in AgamOBP1, as are Phe123 backbone carbonyl and Val125 backbone nitrogen. The C-terminal carboxylate of

Val125 is within hydrogen bond distance of Tyr54, and this hydrogen bond is exposed to the binding pocket solvent.

AgamOBP1 binding channel opens to the solvent through a space created by helices one, three, and four. This opening is bordered by residues Leu15, Ala18, Leu22, Ala62, Val64, and Leu73. Binding pockets of LUSH and Amel-ASP1 also open to solvent through a hole formed by helices one, three and four. In all three cases, residues from the first three turns of helix one, and from the N-termini of helices three and four contribute to forming the opening. In the case of LmaPBP, the opening is on the opposite side of the molecule and is formed by residues on helices 5 and 6, as well as on the loop between helices 3 and 4. With ApolPBP1, there are two openings, one formed by helix 3 and the N-terminal ends of helices 4 and 6, and the other between helix 1a, the C-terminus of helix 6, and the loop between helices 2 and 3.

The opening through the dimer interface is through a hole between helices 4 and 5, and is not present in the opening to solvent of any of the other structurally characterized OBPs. Five residues line this opening: Leu73, His77, Met89, Gly92, and Leu96. In the case of Amel-ASP1, side chains of four of the five homologous residues block this opening: Glu67, Leu71, Gln83, and Met86. AgamOBP1 Leu73 and His77 (homologous to Amel-ASP1 Glu67 and Leu71, respectively) are in alternate rotomer conformation relative to the Amel-ASP1 residues, which move them out of the way of the opening. AgamOBP1 Met89 is in essentially the same rotomer conformation as the homologous residue in Amel-ASP1 (Gln83), but helix five, which contains AgamOBP1 Met89 and Gly92, is shifted roughly 2 Å away from helix four in AgamOBP1 relative to Amel-ASP1. Finally, in addition to being shifted approximately 2 Å, the Amel-ASP1 Met86 side-chain is missing in the homologous residue of AgamOBP1 (Gly92).

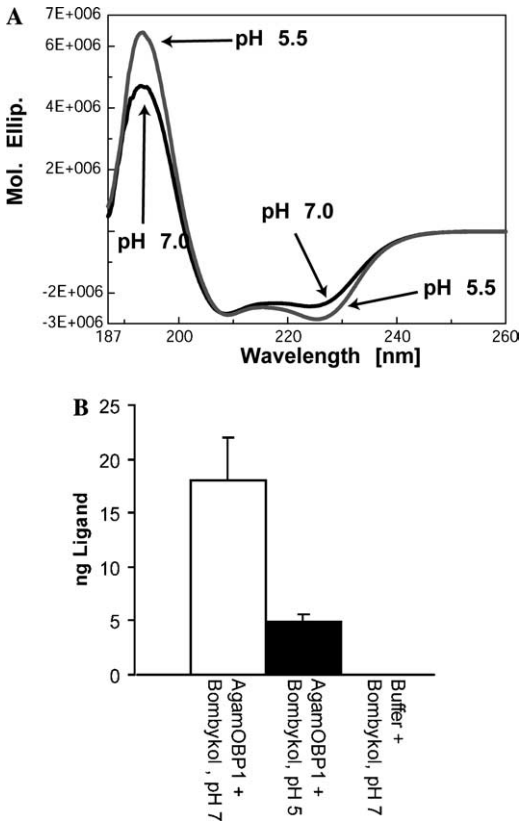

Fig. 4. AgamOBP1 undergoes a pH dependent conformational change that is associated with loss of affinity for ligand. (A) CD spectrum of AgamOBP1 in the absence of ligand at pH 7.0 and pH 5.5. (B) Bombykol was incubated with AgamOBP1. Total bombykol still remaining after filtration and wash is shown. Experiment was run at pH 7.0 (white) or pH 5.5 (black). A no protein control at pH 7.0 was also run (gray). There was no bombykol on the filters in the no protein control. Previous experiments have shown that binding of bombykol to filter is independent of pH [3].

pH dependent conformational changes and binding

Both *B. mori* PBP and ApolPBP1 undergo a pH dependent conformational change that leads to release of pheromone [19,25,26]. We were therefore interested in determining whether AgamOBP1 also undergoes pH dependent changes. CD spectra (Fig. 4A) indicate that AgamOBP1 does, in fact, show conformational changes upon changing pH. We next examined the effect of pH on the ability of AgamOBP1 to bind a ligand. Since the native ligand of AgamOBP1 is unknown, an artificial ligand was used. Bombykol was chosen because its long aliphatic chain was likely to fit in the long hydrophobic binding tunnel of the protein and also because previous studies of bombykol binding to *B. mori* PBP made it a convenient substitute ligand [3]. As seen in Fig. 4B, bombykol binds with significantly lower affinity to AgamOBP1 at pH 5 than at pH 7. This is reminiscent of the pH dependent binding of bombykol to *B. mori* PBP, though the effect is more dramatic in *B. mori* PBP. In the case of *B. mori*, loss of ligand binding at low pH is due to a conformational change in the C-terminal extension. This extension forms a helix that actually occupies the binding pocket of the protein. In the case of AgamOBP, as with LUSH and Amel-ASP1, the C-terminus is too short to form a helix that fits in the binding pocket. However, the AgamOBP1 C-terminus does form a wall of the binding pocket, and this wall is held in place by hydrophobic and polar contacts with the N-terminus and surrounding helices. The majority of the polar contacts between the N and C-terminal loops are between carboxylates and NH groups. For example, in addition to the previously mentioned Tyr54, the C-terminal carboxylate of Val125 also interacts with the δ nitrogen of His23, and this interaction is exposed to bulk solvent. In addition, there are three aspartic acid residues (Asp7, Asp42, and Asp118) that interact with either arginine (Arg5 with Asp7, and Arg6 with Asp42), histidine (His121 with Asp118) or backbone nitrogen (Tyr10 with Asp7). We expect that one or more of these interactions would be disrupted at lower pH, causing these loops to separate. This would leave the binding pocket open to solvent, significantly decreasing the binding affinity of the protein for the ligand.

Discussion

The comparison of the six OBPs whose structures have been solved suggests that three of them—LUSH, AmelASP1, and AgamOBP1—belong to a structural subclass of OBPs [17,18,23–25]. This subclass is distinguished from other OBPs by having a C-terminus that forms a wall of the binding pocket and abuts the N-terminal helix, and by having an opening to the binding pocket that consists of residues from the first three turns of the first helix and the N-termini of the third and fourth helices. At least in the case of AgamOBP1, the structure of the N and C termini may have implications for the functioning of the protein (see below).

A significant difference among the six structures is the presence or absence of a clear dimer interface. Despite evidence that it forms a dimer under certain circumstances (including the pH 8.2 at which crystals form) [38], the crystal structure of PBP from *B. mori* did not show a clear dimer interface, having an interface that was either far too small or non-symmetrical to be a true dimer [18]. On the other hand, both LUSH at pH 4.6 [24] and AgamOBP1 form symmetrical dimers with over 1000 $Å^2$ buried surface. However, the interfaces are not structurally conserved. Thus, there does not appear to be any structurally conserved mechanism by which OBPs form dimers.

The most distinctive feature of AgamOBP1 is the very long hydrophobic tunnel that goes through the dimer interface and is open to solvent on both sides. Such a long feature is surprising in an odorant binding protein, since it can accommodate a chain of at least 40 PEG atoms entirely within the protein cavity (Fig. 3). A fatty acid or aliphatic hydrocarbon alcohol measuring a fraction of this length would be too large to be significantly volatile. Given the large percentage of polar contacts in the interface, it is likely that the protein is largely a monomer in the antennae. However, the actual concentration of AgamOBP1 in vivo is unknown. If the concentration is sufficiently high, then the protein may exist as a dimer in the antennae. If this is so, it is possible that whatever the ligand is that binds to AgamOBP1, it requires the fairly straight binding pocket that is found running through the dimer interface. In this model, the channel from the bend or "elbow" of the channel to the solvent surface would be unoccupied upon ligand binding, leaving only the central portion of the molecule occupied. That is, if the dimer interface is physiological, it might have evolved to accommodate a ligand that binds best in an extended conformation that is too long to fit in a single molecule but not so long as to occupy the whole binding pocket. An alternative hypothesis is that AgamOBP1 binds more than one ligand and does so in different portions of the molecule. Thus, for example, one ligand might bind near the dimer interface while the other binds in the "elbow" (which is analogous to the binding pocket of the other OBPs whose structures have been determined). The different ligands could be bound at different times as the mosquito encounters different odorants or they could bind simultaneously.

Previous work has demonstrated that *B. mori* PBP undergoes a conformational change as pH goes from neutral to low[19]. This change in pH causes the C-terminus to form a helix that actually occupies the binding pocket of the PBP, thus precluding binding of the pheromone bombykol. It has been proposed that this has functional significance for odorant sensing. The model is that bombykol enters the sensillar lymph and is bound by PBP. The complex of PBP and bombykol then diffuses to the negatively charged sensory neuron surface. This negative charge lowers the pH around the neuronal surface, which has the odorant receptors. This lower pH causes a change in PBP conformation that releases bombykol, thereby delivering the pheromone to the receptor. Subsequent OBP structures showed that the C-terminal tail long enough to form a helix was not a feature shared by all OBPs. This suggested, then, that this pH dependent binding and releasing was not a general feature of OBPs. However, current data show that AgamOBP1, which also lacks a C-terminal extension long enough to form a helix that would displace a ligand, does undergo a pH dependent conformational change (Fig. 4A). Furthermore, this conformational change is associated with a decrease in binding ability of the protein. This is consistent with the structural features of AgamOBP1, which show that the predominant polar interactions between the N- and C-terminal loops involve interactions between carboxylates and either asparagines, histidines, or main chain amides. Such interactions are likely to be acid-labile due to the protonation of the carboxylate in low pH. In this case, rather than the C-terminus forming a helix to displace ligand, the C-terminus might move out away from the ligand, thus exposing it to bulk solvent and lowering the affinity of the protein for the ligand. Thus, the crystal structure itself, the CD data, and the binding data all support the concept that AgamOBP1, like *B. mori* PBP and ApolPBP1, undergoes a pH dependent conformational change that lowers affinity for the ligand. Since distantly related OBPs have the same property, it seems likely that this is a more general property of OBPs and is perhaps a common mechanism of odorant delivery to odorant receptors.

Acknowledgments

This work was supported in part by funds from the NIH (GM66135 and 1U01AI058267-01), the National Science Foundation (NSF) (0234769), NIH training Grant T32 GM070377, and the National Research Initiative of the USDA Cooperative State Research, Education, and Extension Service (2003-35302-13468). The data collection facilities at Stanford Synchrotron Radiation Laboratory are funded by the US Department of Energy and the NIH.

References

[1] H.V. Pates, W. Takken, K. Stuke, C.F. Curtis, Differential behaviour of *Anopheles gambiae* sensu stricto (Diptera: Culicidae) to human and cow odours in the laboratory, Bull. Entomol. Res. 91 (2001) 289–296.

[2] L.J. Zwiebel, W. Takken, Olfactory regulation of mosquito–host interactions, Insect Biochem. Mol. Biol. 34 (2004) 645–652.

[3] W.S. Leal, A.M. Chen, Y. Ishida, V.P. Chiang, M.L. Erickson, T.I. Morgan, J.M. Tsuruda, Kinetics and molecular properties of pheromone binding and release, Proc. Natl. Acad. Sci. USA 102 (2005) 5386–5391.

[4] R.G. Vogt, L.M. Riddiford, Pheromone binding and inactivation by moth antennae, Nature 293 (1981) 161–163.

[5] T. Sakurai, T. Nakagawa, H. Mitsuno, H. Mori, Y. Endo, S. Tanoue, Y. Yasukochi, K. Touhara, T. Nishioka, Identification and functional characterization of a sex pheromone receptor in the silkmoth *Bombyx mori*, Proc. Natl. Acad. Sci. USA 101 (2004) 16653–16658.

[6] R.G. Vogt, L.M. Riddiford, G.D. Prestwich, Kinetic properties of a sex pheromone-degrading enzyme: the sensillar esterase of *Antheraea polyphemus*, Proc. Natl. Acad. Sci. USA 82 (1985) 8827–8831.

[7] M. Maibeche-Coisne, A.A. Nikonov, Y. Ishida, E. Jacquin-Joly, W.S. Leal, Pheromone anosmia in a scarab beetle induced by in vivo inhibition of a pheromone-degrading enzyme, Proc. Natl. Acad. Sci. USA 101 (2004) 11459–11464.

[8] Y. Ishida, W.S. Leal, Rapid inactivation of a moth pheromone, Proc. Natl. Acad. Sci. USA 102 (2005) 14075–14079.

[9] E. Plettner, J. Lazar, E.G. Prestwich, G.D. Prestwich, Discrimination of pheromone enantiomers by two pheromone binding proteins from the gypsy moth *Lymantria dispar*, Biochemistry 39 (2000) 8953–8962.

[10] M.S. Kim, A. Repp, D.P. Smith, LUSH odorant-binding protein mediates chemosensory responses to alcohols in *Drosophila melanogaster*, Genetics 150 (1998) 711–721.

[11] R.G. Vogt, The biochemistry of odor detection and its future prospects., in: G.J. Blomquist, and Vogt, R. G. (Ed.), Insect Pheromone Biochemistry and Molecular Biology, The biosynthesis and detection of pheromones and plant volatiles, London, 2003.

[12] W.S. Leal, Proteins that make sense., in: G.J. Blomquist, R.G. Vogt, (Eds.), Insect Pheromone Biochemistry and Molecular Biology, The Biosynthesis and Detection of Pheromones and Plant volatiles, London, 2003.

[13] W.S. Leal, Pheromone reception, Top. Curr. Chem. 240 (2005) 1–36.

[14] P. Xu, R. Atkinson, D.N. Jones, D.P. Smith, *Drosophila* OBP LUSH is required for activity of pheromone-sensitive neurons, Neuron 45 (2005) 193–200.

[15] P. Pelosi, Odorant-binding proteins, Crit. Rev. Biochem. Mol. Biol. 29 (1994) 199–228.

[16] K.E. Kaissling, Olfactory perireceptor and receptor events in moths: a kinetic model, Chem. Senses 26 (2001) 125–150.

[17] A. Lartigue, A. Gruez, S. Spinelli, S. Riviere, R. Brossut, M. Tegoni, C. Cambillau, The crystal structure of a cockroach pheromone-binding protein suggests a new ligand binding and release mechanism, J. Biol. Chem. 278 (2003) 30213–30218.

[18] B.H. Sandler, L. Nikonova, W.S. Leal, J. Clardy, Sexual attraction in the silkworm moth: structure of the pheromone-binding-protein–bombykol complex, Chem. Biol. 7 (2000) 143–151.

[19] R. Horst, F. Damberger, P. Luginbuhl, P. Guntert, G. Peng, L. Nikonova, W.S. Leal, K. Wuthrich, NMR structure reveals intramolecular regulation mechanism for pheromone binding and release, Proc. Natl. Acad. Sci. USA 98 (2001) 14374–14379.

[20] T.A. Keil, Surface coats of pore tubules and olfactory sensory dendrites of a silkmoth revealed by cationic markers, Tissue Cell 16 (1984) 705–717.

[21] H. Wojtasek, W.S. Leal, Conformational change in the pheromone-binding protein from *Bombyx mori* induced by pH and by interaction with membranes, J. Biol. Chem. 274 (1999) 30950–30956.

[22] C.H. Wetzel, H.J. Behrendt, G. Gisselmann, K.F. Stortkuhl, B. Hovemann, H. Hatt, Functional expression and characterization of a *Drosophila* odorant receptor in a heterologous cell system, Proc. Natl. Acad. Sci. USA 98 (2001) 9377–9380.

[23] A. Lartigue, A. Gruez, L. Briand, F. Blon, V. Bezirard, M. Walsh, J.C. Pernollet, M. Tegoni, C. Cambillau, Sulfur single-wavelength anomalous diffraction crystal structure of a pheromone-binding protein from the honeybee *Apis mellifera* L, J. Biol. Chem. 279 (2004) 4459–4464.

[24] S.W. Kruse, R. Zhao, D.P. Smith, D.N. Jones, Structure of a specific alcohol-binding site defined by the odorant binding protein LUSH from *Drosophila melanogaster*, Nat. Struct. Biol. 10 (2003) 694–700.

[25] S. Mohanty, S. Zubkov, A.M. Gronenborn, The solution NMR structure of *Antheraea polyphemus* PBP provides new insight into pheromone recognition by pheromone-binding proteins, J. Mol. Biol. 337 (2004) 443–451.

[26] W.S. Leal, A.M. Chen, M.L. Erickson, Selective and pH-dependent binding of a moth pheromone to a pheromone-binding protein, J. Chem. Ecol. 31 (2005) 2493–2499.

[27] H. Biessmann, M.F. Walter, S. Dimitratos, D. Woods, Isolation of cDNA clones encoding putative odorant binding proteins from the antennae of the malaria-transmitting mosquito, *Anopheles gambiae*, Insect Mol. Biol. 11 (2002) 123–132.

[28] C.R. Kissinger, D.K. Gehlhaar, D.B. Fogel, Rapid automated molecular replacement by evolutionary search, Acta Crystallogr. D Biol. Crystallogr. 55 (Pt 2) (1999) 484–491.

[29] L.C. Storoni, A.J. McCoy, R.J. Read, Likelihood-enhanced fast rotation functions, Acta Crystallogr. D Biol. Crystallogr. 60 (2004) 432–438.

[30] J. Navaza, On the computation of the fast rotation function, Acta Crystallogr. D Biol. Crystallogr. 49 (1993) 588–591.

[31] A.G.W. Leslie, Recent changes to the MOSFLM package for processing film and image plate data, Joint CCP4 + ESF-EAMCB Newsletter on Protein Crystallography 26 (1992).

[32] T.C. Terwilliger, J. Berendzen, Automated MAD and MIR structure solution, Acta Crystallogr. D Biol. Crystallogr. 55 (Pt 4) (1999) 849–861.

[33] T.A. Jones, J.-Y. Zou, S.W. Cowan, M. Kjeldgaard, Improved methods for building protein models in electron density maps and the location of errors in these models, Acta Crystallograph. Section A 47 (1991) 110–119.

[34] A.T. Brunger, P.D. Adams, G.M. Clore, W.L. DeLano, P. Gros, R.W. Grosse-Kunstleve, J.S. Jiang, J. Kuszewski, M. Nilges, N.S. Pannu, R.J. Read, L.M. Rice, T. Simonson, G.L. Warren, Crystallography and NMR system: A new software suite for macromolecular structure determination, Acta Crystallogr. D Biol. Crystallogr. 54 (Pt 5) (1998) 905–921.

[35] D.M. van Aalten, R. Bywater, J.B. Findlay, M. Hendlich, R.W. Hooft, G. Vriend, PRODRG, a program for generating molecular topologies and unique molecular descriptors from coordinates of small molecules, J. Comput. Aid Mol. Des. 10 (1996) 255–262.

[36] R.A. Laskowski, M.W. MacArthur, D.S. Moss, J.M. Thornton, PROCHECK: a program to check the stereochemical quality of protein structures, J. Appl. Crystallogr. 26 (1993) 283–291.

[37] W. Kabsch, A solution for the best rotation to relate two sets of vectors, Acta Crystallogr. A 32 (1976) 922–923.

[38] W.S. Leal, Duality monomer-dimer of the pheromone-binding protein from *Bombyx mori*, Biochem. Biophys. Res. Commun. 268 (2000) 521–529.